Pergamon

Int. J. Heat Mass Transfer. Vol. 38, No. 5, pp. 853–862, 1995

0017-9310/95 $9.50+0.00

0017-9310(94)00199-5

Laminar forced convection in a helicoidal pipe with finite pitch

G. YANG, Z. F. DONG and M. A. EBADIAN†

Department of Mechanical Engineering, Florida International University, Miami, FL 33199. U.S.A.

(*Received* 6 *August* 1993 *and in final form* 1 *July* 1994)

Abstract—This paper presents a numerical investigation of fully developed laminar convective heat transfer in a helicoidal pipe with a finite pitch coiled pipe. Three major parameters are identified to affect laminar convective heat transfer in a helicoidal pipe: the Dean number, torsion and the Prandtl number. The results indicate that torsion will increase the temperature gradient on one side of the pipe wall and decrease the temperature gradient on the other side. In the case of a small Prandtl number fluid, the Nusselt number declines slightly as torsion increases. However, in the case of a large Prandtl number fluid, the Nusselt number is significantly reduced as torsion increases. The predicted results for the limiting cases are also compared with other numerical and experimental results.

INTRODUCTION

Due to their compact structure and high heat transfer coefficient, coiled pipes are used extensively in heat recovery systems, compact heat exchangers, storage tank heating systems, and refrigeration for the chemical, dairy, drug and food industries. Because of interest in their practical applications, numerous investigations have been carried out in this field. However, although many researchers claim that their investigation deals with the helicoidal pipe, their analyses are actually based on the toroidal pipe, since the effect of the coil pitch is absent in them. The pitch of the coil will create a rotation force (torsion force), which may significantly affect the flow pattern. Considering the effects of torsion will dramatically increase the complexity of the study. A survey of the open literature indicates that only a few papers have been published in this area to include the effects of torsion on laminar forced flow in a helicoidal pipe [1–9]. However, none of these papers discusses the effects of torsion on convective heat transfer in a helicoidal pipe, which is the motivation behind the present investigation. For the purpose of distinguishing the terminology, the helicoidal pipe in this study refers to the coiled pipe with finite pitch and the toroidal pipe represents a coiled pipe with zero pitch.

In the toroidal pipe, two symmetrical loops of secondary flow are formed due to centrifugal force [10]. In the helicoidal pipe, torsion will distort the symmetrical loops of the secondary flow. Early studies of helicoidal pipe flow largely relied on experiments [11–13]. A non-orthogonal helicoidal coordinate system was introduced [1] to formulate the Navier–Stokes equation for helicoidal pipe flow, and this problem was eventually solved by applying the perturbation method for the case of small curvature and small torsion. It was concluded that, in the helicoidal pipe, both curvature and torsion can produce a first-order effect on the flow [1]. The Navier–Stokes equations were simplified [2] by assuming a small curvature using a non-orthogonal coordinate system, and it was found that the Dean number is the dominant parameter and that torsion has almost no effect on the axial flow rate. A transformation to render the non-orthogonal coordinate system to an orthogonal one was introduced [3, 4] and it was found that the effect of torsion on the secondary flow is of second order. Germano's coordinate system was used by Kao [5] to study helicoidal pipe flow in a substantial range of Dean numbers using both perturbation and numerical methods and it was found that at certain torsion–curvature ratios, the effect of torsion on secondary flow can reach an order of magnitude of one and a half powers. This study also concluded that, although torsion can significantly change the secondary flow pattern in a helicoidal pipe, the axial flow rate varies only slightly. An attempt was made [6] to resolve the controversy between the above-mentioned research [1, 3] by linking Wang's coordinate system with Germano's coordinate system. A detailed comparison was made [7] between the non-orthogonal and orthogonal coordinates of refs. [1] and [3], and it was noted that the torsion effect on secondary flow in the helicoidal pipe depends on the frame of reference of the observer. Fully developed laminar flow in the helical pipe with a circular cross section was also investigated in that work by using the equation formulated by Germano [3, 4], except for minor changes in the nomenclature, and it was verified that torsion has a first-order effect. Recently, the double series expansion method was used [8], which perturbs the exact solution of a twisted

†Author to whom correspondence should be addressed.

NOMENCLATURE

a	pipe diameter [m]
De	Dean number
f	friction factor, equation (9)
f_c	friction coefficient for a curved pipe
f_s	friction coefficient for a straight pipe
Nu	local Nusselt number, Fig. 8
Nu_c	average Nusselt number for a curved pipe
Nu_h	average Nusselt number for the helicoidal pipe, equation (10)
Nu_s	average Nusselt number for the straight pipe
P	dimensionless pressure
Pr	Prandtl number
p	pitch
p^*	dimensionless pressure [Pa]
R	radius of the coil [m]
Re	Reynolds number, equation (6)
r	dimensionless radial direction coordinate
r^*	dimensional radial direction coordinate [m]
s	dimensionless axial coordinate
s^*	dimensional axial coordinate [m]
T	dimensionless temperature
T^*	fluid temperature [K]
T_b	bulk temperature [K]
T_b^*	dimensional bulk temperature [K]
T_w	wall temperature [K]
u, v, w	dimensionless velocity components $(u^*, v^*, w^*)/(\nu/a)$
u^*, v^*, w^*	velocity components in the ψ, r and s directions [m s^{-1}]
w_b	dimensionless average axial velocity
w_b^*	dimensional average axial velocity [m s^{-1}].

Greek symbols

ε	dimensionless curvature, κa
θ	angle
κ	curvature [m^{-1}]
λ	dimensionless torsion, τ/κ
ν	kinematic viscosity [m^2 s^{-1}]
ρ	density [kg m^{-3}]
τ	torsion; shear stress
ψ	angle
ω	function, equation (7).

Subscripts

r	radial direction
s	axial direction
ψ	tangential direction.

circular pipe to obtain the solution of the helicoidal pipe. The perturbed parameters are dimensional curvature, κ, and dimensional torsion, τ. It was concluded that inconsistency of the torsion effect on the secondary flow between [1] and [3, 4] can be quantitatively explained by the different coordinate systems used. None of the above mentioned research dealt with laminar convective heat transfer in a helicoidal pipe with a finite pitch coiled pipe.

Numerous studies have been conducted to examine heat transfer behavior in the curved pipe [14–23]. Excellent reviews can be found in refs. [24–30]. It must be emphasized here that, in many theoretical and numerical studies, the researchers have claimed they considered the effect of pitch on convective heat transfer in a helicoidal pipe. However, inspection of their equations reveals that either only part of the effect of torsion is considered, or an improper expression for the torsion term is applied. For example, a modification was made [31] in the formulation of the toroidal coordinate system to predict the pitch effect by simply replacing the original axial velocity by the product of the axial velocity and the inclination angle. In that solution, therefore, the axial velocity and temperature distributions for the case of pure forced convection are retained in the symmetry no matter what pitch value is used, which is physically unreasonable. Recently, Yang *et al.* [32] studied the heat transfer behavior in a helicoidal pipe. The objective of the present paper is to explore the effects of torsion on laminar forced convective heat transfer in a helicoidal pipe with a finite pitch coil. The flow is assumed to be hydrodynamically and thermally fully developed with constant fluid properties, and the effects of free convection are neglected. Uniform axial heat flux with a peripheral constant wall temperature boundary condition is applied in this investigation.

PROBLEM FORMULATION

Consider a helicoidal pipe with diameter, $2a$, coil diameter, $2R$, curvature, κ, and considerable pitch, p, as shown in Fig. 1. The steady laminar flow of incompressible Newtonian fluid in the helicoidal pipe is assumed to be hydrodynamically and thermally fully developed. The fluid properties are independent of the temperature. The helicoidal pipe is subjected to a thermal boundary condition of uniform axial wall heat flux with a uniform peripheral wall temperature. The coordinate system of [4] is applied here. In Fig. 1, s^*, r^* and ψ indicate the dimensional axial coordinates, where $\psi = \theta + \phi$ and

$$\phi(s^*) = \int_{s_0}^{s^*} \tau(s)\, \mathrm{d}s'.$$

As noted by refs. [4] and [7], the helical coordinate systems (r^*, ψ, s^*) are orthogonal systems for fully

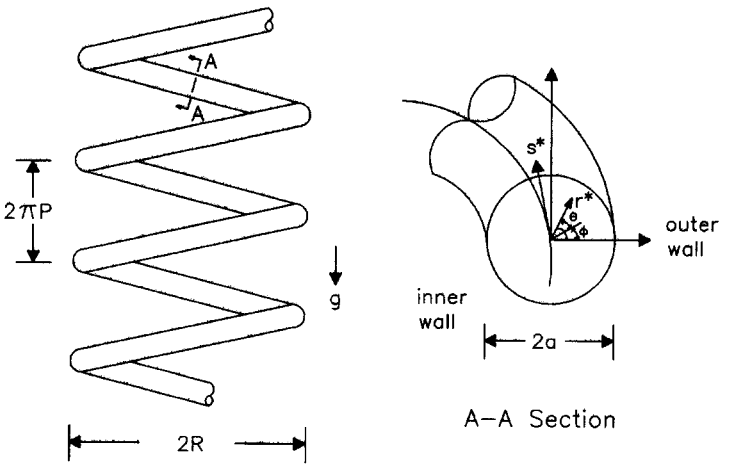

$$\kappa = \frac{R}{R^2 + P^2} \qquad \tau = \frac{P}{R^2 + P^2}$$

Fig. 1. A schematic representation of a helicoidal pipe.

developed laminar flow without consideration of viscous dissipation and the effect of free convection. The continuity, momentum, and energy equations can be written in the following dimensionless form;

$$\frac{1}{r}\frac{\partial u}{\partial \psi} + \frac{\partial v}{\partial r} + \frac{v}{r} + \varepsilon\omega\left[u\cos\psi + v\sin\psi - \lambda\frac{\partial w}{\partial \psi}\right] = 0 \tag{1}$$

$$\begin{aligned}
&\frac{\partial(uu)}{r\,\partial\psi} + \frac{1}{r}\frac{\partial(ruv)}{\partial r} = -\frac{1}{r}\frac{\partial p}{\partial \psi} \\
&+\varepsilon w\omega\left(w\cos\psi + \lambda\frac{\partial u}{\partial \psi}\right) - \frac{uv}{r} \\
&-u\varepsilon\omega\left[u\cos\psi + v\sin\psi - \lambda\frac{\partial w}{\partial \psi}\right] \\
&+\frac{1}{r}\frac{\partial}{\partial r}(r\tau_{r\psi}) + \frac{\partial}{r\,\partial\theta}(\tau_{\psi\psi}) \\
&+\frac{\tau_{r\psi}}{r} + \varepsilon\omega(\tau_{\psi\psi}\cos\psi + \tau_{r\psi}\sin\psi + \tau_{ss}\cos\psi) \\
&-\varepsilon\omega\lambda\frac{\partial}{\partial \psi}(\tau_{\psi s})
\end{aligned} \tag{2}$$

$$\begin{aligned}
&\frac{1}{r}\frac{\partial(uv)}{\partial\psi} + \frac{1}{r}\frac{\partial(rvv)}{\partial r} = -\frac{\partial P}{\partial r} \\
&+\frac{1}{r}\frac{\partial(r\tau_{rr})}{\partial r} + \frac{1}{r}\frac{\partial(\tau_{r\psi})}{\partial\psi} \\
&+\varepsilon\omega w\left(w\sin\psi + \lambda\frac{\partial v}{\partial\psi}\right) + \frac{u^2}{r} \\
&-v\varepsilon\omega\left[u\cos\psi + v\sin\psi - \lambda\frac{\partial w}{\partial\psi}\right] \\
&-\frac{\tau_{\psi\psi}}{r} + \varepsilon\omega(\tau_{r\psi}\cos\psi + \tau_{rr}\sin\psi - \tau_{ss}\sin\psi) \\
&-\varepsilon\omega\lambda\frac{\partial}{\partial\psi}(\tau_{rs})
\end{aligned} \tag{3}$$

$$\begin{aligned}
&\frac{\partial(uw)}{r\,\partial\psi} + \frac{1}{r}\frac{\partial(rvw)}{\partial r} = -\omega\frac{\partial p}{\partial s} \\
&-2w\varepsilon\omega\left[u\cos\psi + v\sin\psi - \lambda\frac{\partial w}{\partial\psi}\right] \\
&+\frac{1}{r}\frac{\partial}{\partial\psi}(\tau_{\psi s}) + \frac{1}{r}\frac{\partial}{\partial r}(r\tau_{rs}) \\
&+2\varepsilon\omega(\tau_{\psi s}\cos\psi + \tau_{rs}\sin\psi)
\end{aligned} \tag{4}$$

$$\begin{aligned}
&\frac{u}{r}\frac{\partial T}{\partial\psi} + v\frac{\partial T}{\partial r} - \omega\frac{w}{w_b} - \omega\varepsilon\lambda w\frac{\partial T}{\partial\psi} \\
&= \frac{1}{Pr}\left[\frac{\partial^2 T}{\partial r^2} + \frac{1}{r}\frac{\partial T}{\partial r} + \frac{1}{r^2}\frac{\partial^2 T}{\partial\psi^2}\right. \\
&+\varepsilon\omega\left(\sin\psi\frac{\partial T}{\partial r} + \cos\psi\frac{1}{r}\frac{\partial T}{\partial\psi}\right) \\
&+\omega^2\left(\varepsilon^2\lambda^2\frac{\partial^2 T}{\partial\psi^2} + \lambda^2\varepsilon^3 r\omega\cos\psi\frac{\partial T}{\partial\psi}\right. \\
&\left.\left.-\frac{2}{Re}\lambda\varepsilon^2 r\cos\psi\right)\right].
\end{aligned} \tag{5}$$

In equations (2)–(4), τ represents the shear stress, which can be expressed in terms of velocity gradients and fluid viscosity. In the above equations, the dimensionless variables are defined as follows:

$$\tau_{\psi\psi} = 2\left(\frac{1}{r}\frac{\partial u}{\partial\psi} + \frac{v}{r}\right)$$

$$\tau_{rr} = 2\left(\frac{\partial v}{\partial r}\right)$$

$$\tau_{ss} = 2\left(-\omega\varepsilon^2\lambda\frac{\partial w}{\partial\psi} + \omega\varepsilon u\cos\psi + \omega\varepsilon v\sin\psi\right)$$

$$\tau_{\psi r} = \left[\frac{1}{r}\frac{\partial v}{\partial\psi} + r\frac{\partial}{\partial r}\left(\frac{u}{r}\right)\right]$$

$$\tau_{rs} = \left(\frac{\partial w}{\partial r} - \omega\varepsilon w\sin\psi - \omega\varepsilon\lambda\frac{\partial v}{\partial\theta}\right)$$

$$\tau_{\psi s} = \left(-\omega\varepsilon^2\lambda\frac{\partial u}{\partial\psi} + \frac{1}{r}\frac{\partial w}{\partial\psi} - \omega\varepsilon w\cos\psi\right) \quad (6)$$

$$r = \frac{r^*}{a} \quad s = \frac{s^*}{a} \quad u = \frac{u^*}{\nu/a} \quad v = \frac{v^*}{\nu/a} \quad w = \frac{w^*}{\nu/a}$$

$$P = p^*/(\rho\nu^2/a^2) \quad \varepsilon = \kappa a \quad \lambda = \frac{p}{R}$$

$$T = \left(\frac{T^* - T_w^*}{a^2 w_b^*/\nu}\right)\Big/\left(-\frac{\mathrm{d}T_b^*}{\mathrm{d}s^*}\right) \quad Re = \frac{w_b(2a)}{\nu}$$

$$De = Re\,\varepsilon^{1/2} \quad \omega = \frac{1}{1+\varepsilon r\sin\psi} \quad (7)$$

T_w and T_b are the wall and fluid bulk temperatures, respectively. They are the function of the s location. The associated boundary conditions for equations (1)–(5) are

$$@ \quad r = 1 \quad u = 0 \quad v = 0 \quad w = 0 \quad T = 0. \quad (8)$$

For fully developed laminar flow, the friction coefficient and average Nusselt number can be expressed as

$$fRe = 2\frac{\mathrm{d}P}{\mathrm{d}s}\Big/ w_b \quad (9)$$

$$Nu_h = Pr/T_b \quad (10)$$

where w_b and T_b are the bulk axial velocity and bulk temperature, respectively, and are defined by

$$w_b = \frac{1}{\pi}\int_0^{2\pi}\int_0^1 wr\,\mathrm{d}r\,\mathrm{d}\theta \quad (11)$$

$$T_b = \frac{1}{\pi w_b}\int_0^{2\pi}\int_0^1 wTr\,\mathrm{d}r\,\mathrm{d}\theta. \quad (12)$$

SOLUTION METHODOLOGY

Since the helicoidal pipe can be viewed as a combination of curved and twisted pipes, the fluid flow is no longer symmetric. Therefore, the entire cross section of a helicoidal pipe is used as the solution domain. A uniform grid is generated in both the r and ψ directions. The governing equations, (1)–(5), are approximated with finite difference equations by the control volume-based finite difference method for u, v, w and T. The convection–diffusion terms are discretized by a power-law scheme [21]. The remaining terms in the governing equations are approximated by the central difference method, which is a scheme for secondary accuracy. A staggered grid system is employed for the velocity components, u and v. The SIMPLE algorithm is applied to handle these equations. Since equations (1)–(4) are independent of temperature, they can be solved together first. When a convergent solution for velocities is reached, equation (5) is then solved to obtain the temperature profile, and the Nusselt number is calculated. The convergence criterion of

$$\frac{\|\Phi_{ij}^{k+1} - \Phi_{ij}^{k}\|_\infty}{\|\Phi_{ij}^{k+1}\|_\infty} \leqslant 10^{-5} \quad (13)$$

is employed for all nodes, where Φ refers to u, v, w and T. Subscript, ij, represents the arbitrary nodes, and superscript, k, represents the kth iteration.

A computer code was developed based on the above-mentioned solution methodology. In order to verify the accuracy of the computer code, the predicted results have been compared with those available in the open literature. As mentioned in the introduction, no data were found in the open literature for laminar convective heat transfer in a helicoidal pipe with a finite pitch coil. Therefore, the following two comparisons are provided in this study: (1) the friction coefficient for the helicoidal pipe and (2) the Nusselt number for the toroidal pipe. An experimental study was conducted [33] on helicoidal pipe flow with an appreciable range of curvature and torsion. It was found that torsion has almost no effect on the friction coefficient, and all test data can be presented by one equation in the laminar region:

$$\frac{f_c}{f_s} = 1 + 0.033\left[\log_{10}\left(\frac{De\,Re}{\mathrm{d}P/\mathrm{d}s}\right)\right]^{4.0}. \quad (14)$$

A comparison of our predicted results with equation (14) and refs. [33, 34] is given in Fig. 2. The predicted numerical results agree well with the results of the correlation equation. Figure 3 is a comparison of the fully developed average Nusselt numbers for the toroidal pipe. The lines indicate our predicted results. The solid circle, square, and triangle indicate the experimental and predicted results by refs. [34, 23, 15] for the case of $Pr = 5$. The hollow circle, square and triangle indicate the results by refs. [34, 23, 16] for the case of $Pr = 0.7$. Good agreement exists between our predictions and the results of the other researchers.

A grid refinement study is also conducted in the present analysis to determine an adequate grid distribution. Uniform grid distributions (angular direction grids × radial direction grids) of 20×20, 30×30, 40×40, 60×60 and 80×80 were tested. Table 1 is a comparison of the predicted results for fully developed Nusselt numbers at different grid distributions. An axial pressure gradient of $\mathrm{d}P/\mathrm{d}s = -3000$, curvature of $\varepsilon = 0.2$ and Prandtl number of $Pr = 1.0$ were applied during the calculation. With the solution of 30×30, 40×40 and 60×60, the values of Re, De, f and Nu at zero grid size have also been predicted by the Richardson extrapolation method [36]. The table

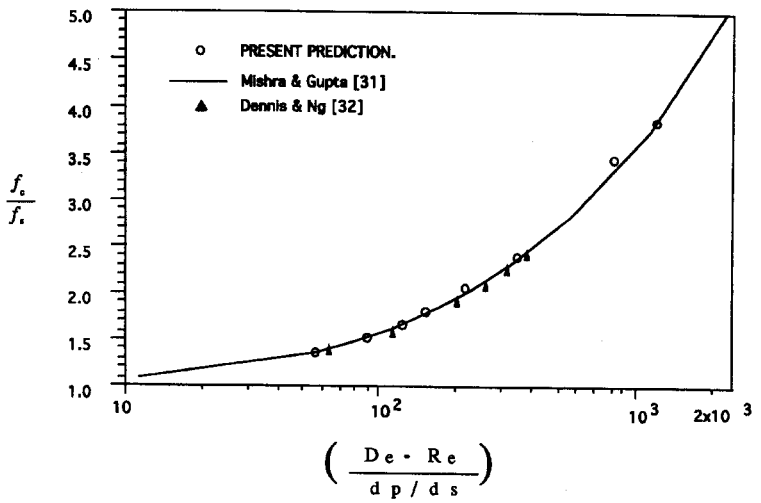

Fig. 2. comparison of the dimensionless friction coefficient.

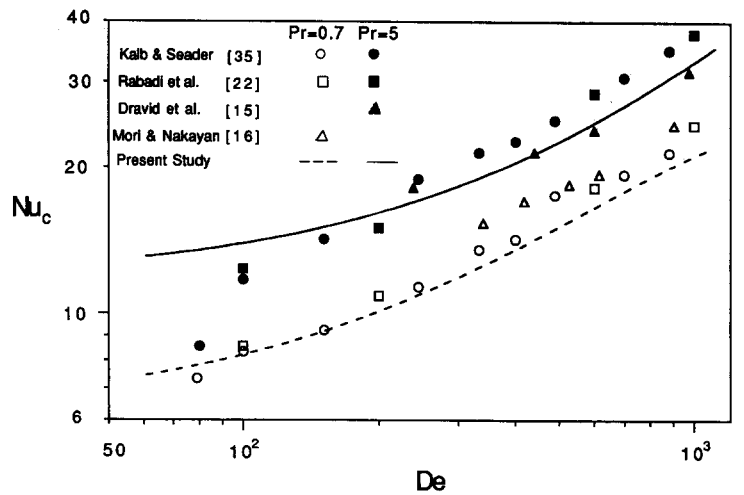

Fig. 3. Comparison of the average Nusselt number vs the Dean number for a curved pipe.

indicates that the 40×40 grid arrangement ensures a satisfactory solution, and the results presented in this paper are based on the calculation of the 40×40 grid size distribution.

RESULTS AND DISCUSSION

One can observe from the governing equations that dimensionless parameters, ε, λ, dP/ds and Pr, are independent variables affecting the characteristics of fluid flow and heat transfer in a helicoidal pipe. According to the definition used in this study, Re and De (defined by $Re\,\varepsilon^{1/2}$), is a dependent variable during the numerical calculations. Generally speaking, the temperature distribution in a helicoidal pipe is largely dependent on the secondary flow pattern in the cross section. Therefore, the secondary flow pattern and the temperature contour will be discussed simultaneously. Figure 4 shows the vector plot for secondary flow at a different λ subject to the conditions of $De = 140$ and $\varepsilon = 0.2$. In each of the figures, the left side indicates the inner wall, and the right side refers to the outer wall of the helicoidal pipe. This definition is also applied to all other figures. Figure 5 indicates the temperature distribution affected by torsion, which is obtained under the same conditions as in Fig. 4.

Table 1. The predicted results and changes with grid arrangements

$L \times M$	Re	De	f	Nu_h
20×20	388.4	173.7	31.2	11.58
30×30	391.8	175.2	30.9	11.39
40×40	391.0	174.8	31.0	11.26
60×60	389.9	174.4	31.1	11.24
Zero grid size	389.6	173.6	31.3	11.24

When $\lambda = 0$, the coil pitch is equal to zero. This indicates that the helicoidal pipe will be the same as a toroidal pipe. Figure 4(a) shows that two symmetrical vortices exist in the cross section. The flow is directed from the inner wall towards the outer wall in the center

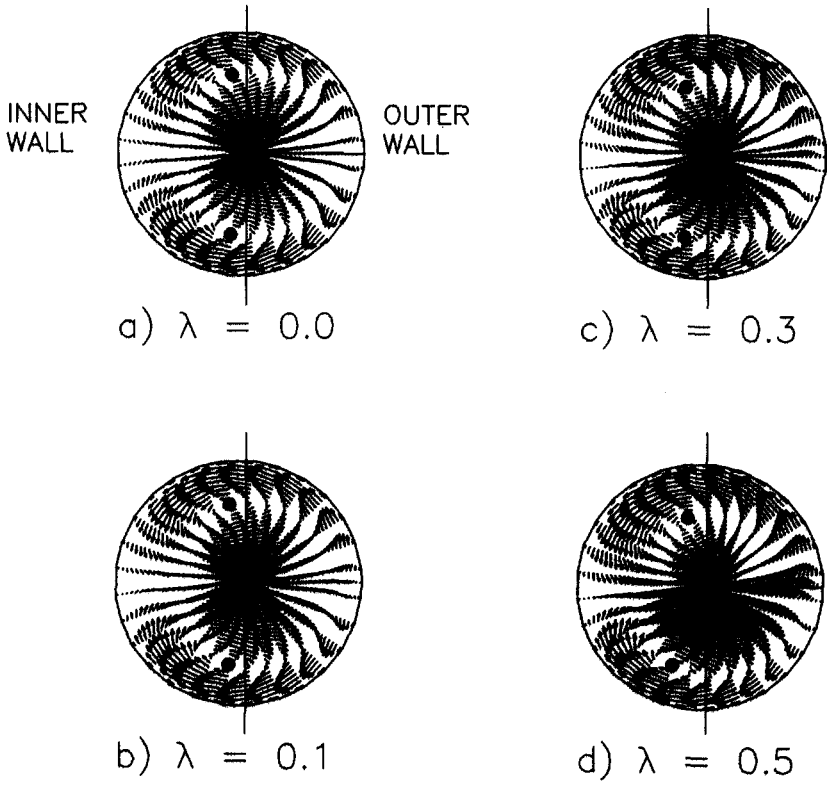

Fig. 4. The secondary flow pattern for $De = 140$ and $\varepsilon = 0.2$.

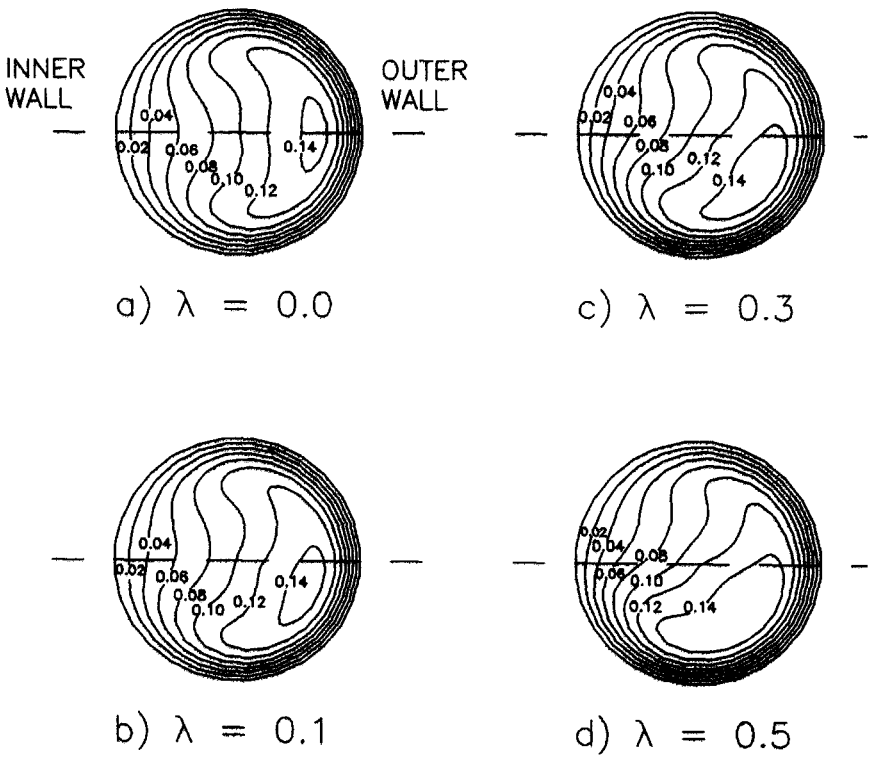

Fig. 5. The temperature distribution in the helicoidal pipe for $De = 140$, $\varepsilon = 0.2$ and $Pr = 1.0$.

region and then returns to the inner wall along the top and bottom of the walls. Figure 5(a) indicates the corresponding temperature distribution. Since the temperature of the wall is lower than that of the fluid, the temperature of the fluid returning along the solid walls to the inner wall is lower. This low temperature fluid is then carried into the interior of the pipe along the centerline. As a result, the high temperature isothermal contours are pushed toward the outer wall. However, the temperature contours remain symmetrical to the centerline in this case, as seen in Fig. 5(a).

Figure 4(b)–(d) exhibits the secondary flow pattern in the helicoidal pipe with a finite coil pitch. In this case, $\lambda \neq 0$, and it can be observed that the two vortices of the secondary flow become asymmetrical. One vortex is enlarged and the other shrinks. For example, when $\lambda = 0.5$, the top vortex in Fig. 4(d) is much larger than the bottom one. It is worthwhile to note the movement of the "eyes" of the two vortices. When $\lambda = 0.1$, the location of the "eyes" is almost unchanged compared with Fig. 4(a). As λ increases, Fig. 4(c) and (d) shows that both "eyes" have moved toward the inner wall. However, the "eye" of the bottom vortex moves much faster than the "eye" of the top vortex. This is due to the bottom vortex becoming weaker than the top vortex. Figure 5(b)–(d) indicates the corresponding temperature contours. Comparing with Fig. 5(a), these figures indicate that the isothermal contours turn clockwise when torsion is applied. This is primarily due to the fact that the additional rotation of the secondary flow created by torsion pushes the high temperature region downward and rotates as well. In fact, the larger the λ, the larger the angle of rotation. For example, at $\lambda = 0.5$, the centerline of the high temperature contours is no longer coincident with the centerline, but in this case, it is approximately 70 degrees from the centerline.

Figure 6 shows the effects of the Dean number on the temperature distributions in the cross section of the helicoidal pipe in the case of $Pr = 1.0$ and $\lambda = 0.1$. The Dean number changes from 40 to 180. It is seen from this figure that the high temperature contours are pushed to the outer wall due to centrifugal force. As the Dean number increases, the contours rotate at a large angle from the centerline and distorts the symmetry. The dashed line in the figure is drawn to represent the pseudo-symmetrical line of the isothermal contour. It seems that the deviation angle of the pseudo-symmetrical line from the horizontal symmetrical line of the pipe becomes larger as the Dean number increases. The Nusselt number, shown in Table 2, indicates that it is a function of De and λ. For purposes of comparison, the Nusselt number for the fully developed straight pipe with an (H1) boundary condition, $Nu = 4.36$, is used as a reference value. It can be seen from Table 2 that the Nusselt number significantly increases as the Dean number increases. At a small Dean number, increasing λ can slightly reduce the peripheral average Nusselt number. In moderate ranges of the Dean number, a sizeable decrease in the Nusselt number can be observed with a large λ. For example, the Nu is reduced almost 8% for the case of $De = 180$ and $\lambda = 0.3$. As the Dean number increases, the temperature gradient near the outer wall region will increase and decrease near the inner wall region. As torsion is applied, the temperature gradient will increase near the bottom half of the wall and decrease near the top half wall region compared with the case without torsion. However, the heat transfer increase (a higher temperature gradient in the wall region) in the bottom half cannot compensate for the decrease in the top half. This results in the overall Nusselt number decrease. As the Dean number increases, this imbalance of the heat transfer between the top and bottom wall region will increase. This results in the torsion effect on the Nusselt number increase as the Dean number increases.

The effects of the Prandtl number on the temperature distribution are depicted in Fig. 7. The Dean number remains at 140 and $\lambda = 0.1$. A corresponding secondary flow pattern can be seen in Fig. 4. An elliptical-type isothermal contour is observed in Fig. 7(a) when $Pr = 0.2$. The temperature gradient on the outer wall is higher than the inner wall, and this nonuniformity of the temperature gradient is not significant. When the Prandtl number is equal to 1.0, the isotherms deform into a moon-like shape. In this case, the isotherms rotate clockwise. The maximum temperature gradient appears at a location at the bottom part of the outer wall. However, when $Pr = 5.0$, the moon-like isotherms distort and two crescent-shaped isotherms appear. This is the result of cold fluid withdrawing from the inner wall to the outer wall. Therefore, the temperature gradient at the top and bottom of the helicoidal pipe is greater, except for the outer wall. As the Prandtl number increases further, two more definite crescent shaped isotherms appear in the cross section of the helicoidal pipe. The temperature gradient at the inner wall increases obviously in this case. In addition, one can observe from an overview of Fig. 7(a)–(d) that the temperature gradient on the wall increases as the Prandtl number increases. Therefore, the Nusselt number is larger when the fluid has a larger Prandtl number. Table 3 shows the effect of the Prandtl number on the Nusselt number at different λ. No matter what value λ is, the Nusselt number increases as the Prandtl number increases. However, when the Prandtl number is less than 1, the Nusselt number is slightly reduced as λ increases, but it reduces even more with a larger Prandtl number. This is attributed to the temperature distribution in the cross section, especially near the wall. In the case of a larger Prandtl number, the temperature gradient at the wall of the bottom half of the pipe is enhanced, but the temperature gradient at the top half of the pipe is remarkably reduced, especially with a larger λ value. As a result, the overall number decreases as the λ value increases.

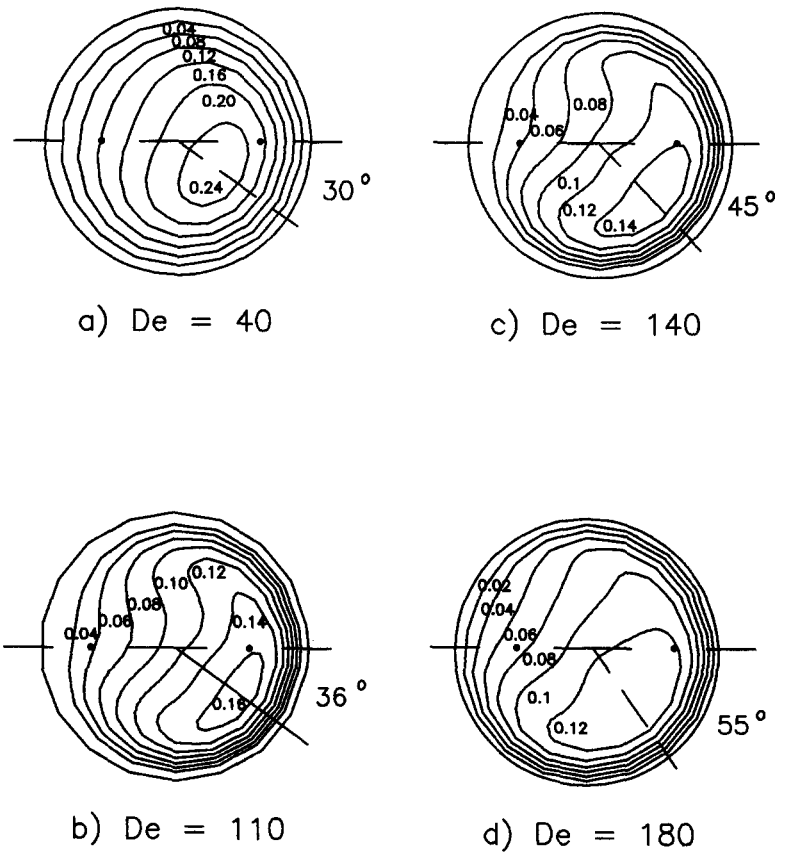

Fig. 6. The effect of the Dean number on the isotherms at $Pr = 1.0$ and $\lambda = 0.3$.

In Fig. 8, the local Nusselt number distribution along the circumference of the helicoidal pipe is displayed for the case of $De = 140$ and $Pr = 5$. The parameter, λ, varies from 0 to 0.3. It is clearly seen that, when $\lambda = 0$, the distribution of the Nusselt number is symmetric, the minimum value of the Nusselt number is located at the inner wall, and the maximum value is at the outer wall. The Nusselt number decreases along the boundary from the outer wall to the inner wall. This is a typical characteristic of the toroidal pipe. However, when $\lambda \neq 0$, the Nusselt number is no longer distributed symmetrically. The location of the minimum Nusselt number shifts upward at the inner wall, although the value of the minimum Nusselt number is nearly the same for different λ. In addition, not only does the value of the maximum Nusselt number increase as λ increases, but its location also shifts downward at the outer wall. It is further seen that the value of the local Nusselt number at each location (ψ) decreases as λ increases on the boundary from 0° to 180°, but, on most of the boundary for 180°–360°, the local value of the Nusselt number increases as λ increases. This means that the Nusselt number on the upper half of the helicoidal pipe decreases and the one on the bottom half increases as λ increases. However, the range of increase is less than the range of decrease.

Table 2. Nusselt number enhancement in a helicoidal pipe

	Nu_h/Nu_s		
De	$\lambda = 0$	$\lambda = 0.1$	$\lambda = 0.3$
0	1	—	—
40	1.357	1.350	1.329
110	2.046	2.025	1.995
140	2.306	2.280	2.202
180	2.622	2.591	2.416

Table 3. Prandtl number effect on the Nusselt number ($Nu_s = 4.36$ is used as a reference value)

	Nu_h/Nu_s		
Pr	$\lambda = 0$	$\lambda = 0.1$	$\lambda = 0.3$
0.2	1.450	1.445	1.443
1	2.306	2.280	2.202
5	3.554	3.378	2.890
10	4.278	3.908	2.970

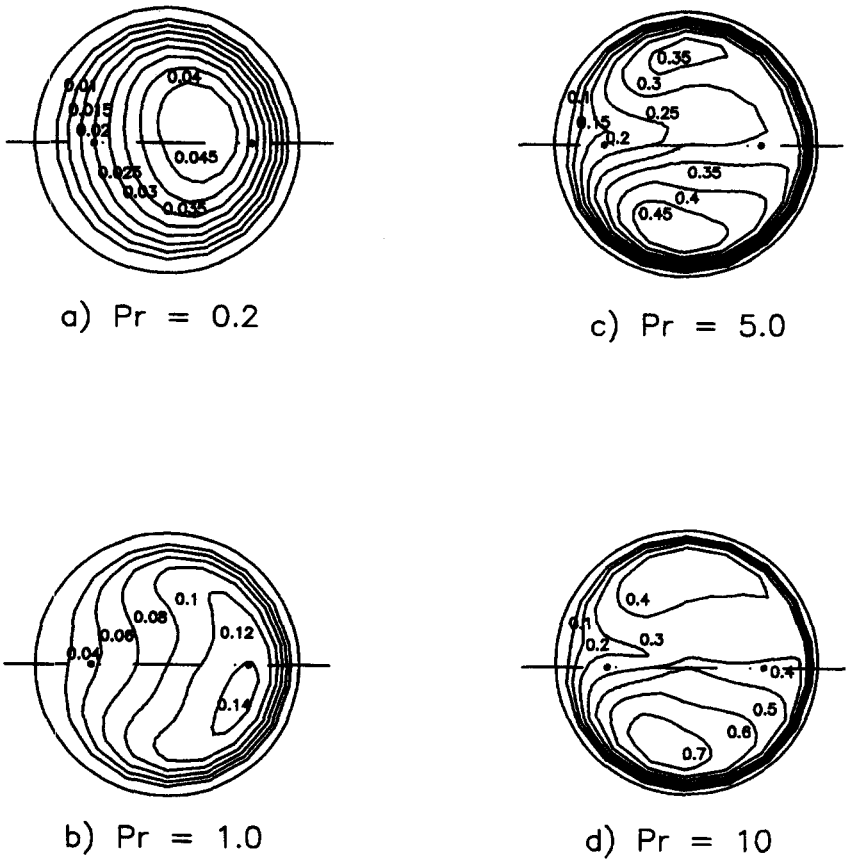

Fig. 7. The effect of the Prandtl number on the isotherms at $De = 140$ and $\lambda = 0.1$.

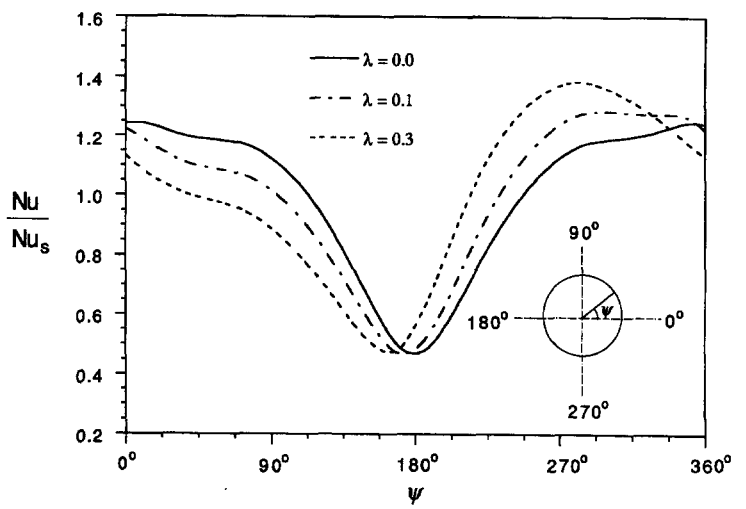

Fig. 8. Local Nusselt number distribution for $De = 140$ and $Pr = 5.0$.

Therefore, the average value of the Nusselt number decreases as λ increases.

CONCLUSIONS

Convective heat transfer of fully developed laminar flow in a finite pitch helicoidal pipe is numerically studied in this paper. The energy equation for helicoidal pipe flow is derived based on the basic law of energy conservation. The heat transfer behavior in a helicoidal pipe is significantly affected by three major parameters: De, λ and Pr. It is concluded that the secondary flow is stronger when the Dean number increases. In this case, a high temperature gradient appears near the outer wall of the helicoidal pipe. However, rotation of the temperature distribution is

attributed to the effect of torsion. As λ increases, a more obvious rotation occurs in the cross section. The shape of the isotherms is also deformed by the torsion effect. This is more significant with a larger Prandtl number flow. The temperature gradient (or local Nusselt number) near the bottom half of the pipe increases markedly and the one near the top half of the pipe decreases. On the other hand, the average Nusselt number increases as the Dean number and the Prandtl number increase, but, as λ increases, the average Nusselt number decreases slightly when Pr is less than 1, and declines significantly with a larger Prandtl number fluid.

Acknowledgement—The results presented in this paper were obtained in the course of research sponsored by the National Science Foundation under Grant No. CTS-9017732.

REFERENCES

1. C. Y. Wang, On the low-Reynolds number flow in a helical pipe, *J. Fluid Mech.* **108,** 185–194 (1981).
2. S. Murata, Y. Miyake, T. Inaba and H. Ogawa, Laminar flow in a helically coiled pipe, *Bull. JSME* **24,** 355–362 (1981).
3. M. Germano, On the effect of torsion in a helical pipe flow, *J. Fluid Mech.* **125,** 1–8 (1982).
4. M. Germano, The Dean equations extended to a helical pipe flow, *J. Fluid Mech.* **203,** 289–356 (1989).
5. H. C. Kao, Torsion effect on fully developed flow in a helical pipe, *J. Fluid Mech.* **184,** 335–356 (1987).
6. D. G. Xie, Torsion effect on secondary flow in a helicoidal pipe, *Int. J. Heat Fluid Flow* **111**(2), 114–119 (1990).
7. E. R. Tuttle, Laminar flow in twisted pipes, *J. Fluid Mech.* **219,** 545–570 (1990).
8. W. Chen and R. Jan, The characteristics of laminar flow in helicoidal circular pipes, *J. Fluid Mech.* **44,** 241–256 (1992).
9. S. Liu and J. H. Masliyah, Axially invariant laminar flow in helical pipes with a finite pitch, *J. Fluid Mech.* **251,** 315–353 (1993).
10. W. R. Dean, Note on the motion of fluid in a curved pipe, *Phil. Mag.* **4,** 208–223 (1927).
11. C. M. White, Streamline flow through curved pipes, *Proc. R. Soc. A* **123,** 645–663 (1929).
12. M. Adler, Stromung in gekrummten rohren, *Z. Angew. Math. Mech. (ZAMM)* **14**(5), 257–275 (1934).
13. H. Ito, Friction factor for turbulent flow in curved pipes, *J. Basic Engng Ser. D* **81,** 123–134 (1959).
14. G. Woschni, Untersuchung des Wärmeubergangs und des Druckverlusts in gekrummten Rohren, Dr.-Ing. Diss., TH, Dresden (1959).
15. E. F. Schmidt, Wärmeubergang und nicht iso-thermer Druckverlust bei erzungener Strömung in schraubenformig gekrummten Rohren, Dr.-Ing. Diss., TH, Braunschweig (1966).
16. A. N. Dravid, K. A. Smith, E. W. Merrill and P. L. T. Brain, Effect of secondary fluid motion on laminar flow heat transfer in helically coiled tubes, *A.I.Ch.E. Jl* **17,** 1114–1122 (1971).
17. Y. Mori and W. Nakayama, Study on forced convective heat transfer in curved pipes, *Int. J. Heat Mass Transfer* **8,** 67–82 (1965).
18. S. P. N. Singh and K. J. Bell, Laminar flow heat transfer in a helically-coiled tube, *Proceedings Fifth International Heat Transfer Conference*, Tokyo, Paper FC53, pp. 193–197 (1974).
19. L. A. M. Jansen and C. J. Hoogendoorn, Laminar convective heat transfer in helical coiled tubes, *Int. J. Heat Mass Transfer* **21,** 1197 (1978).
20. J. M. Tarbell and M. R. Samuels, Momentum and heat transfer in helical coils, *Chem. Engng J.* **5,** 117–127 (1973).
21. S. V. Patankar, *Numerical Heat Transfer and Fluid Flow.* Hemisphere, Washington, DC (1980).
22. M. Akiyama and K. C. Cheng, Laminar forced convection heat transfer in curved pipes with uniform wall temperature, *Int. J. Heat Mass Transfer* **15,** 1426–1431 (1974).
23. N. J. Rabadi, J. C. F. Chow and H. A. Simon, An efficient numerical procedure for the solution of laminar flow and heat transfer in coiled tubes, *Numer. Heat Transfer* **2,** 279–289 (1979).
24. P. S. Srinivasan, S. S. Nandapurkar and F. A. Holland, Pressure drop and heat transfer in coils, *Chem. Engng* 113–119 (May 1968).
25. S. A. Berger, L. Talbot and L. S. Yao, Flow in curved pipes, *A. Rev. Fluid Mech.* **15,** 461–512 (1983).
26. V. Gnielinski, Correlations for the pressure drop in helically coiled tubes, *Int. Chem. Engng* **26**(1), 36–44 (1986).
27. U. Baumeister and H. Brauer, Laminar flow and heat transfer in helically and spirally coiled tubes, *VDI Forschungsheft* No. 593, 2–48 (1979).
28. R. K. Shah and S. D. Joshi, Convective heat transfer in curved ducts. In *Handbook of Single-Phase Convective Heat Transfer* (Edited by S. Kakac, R. K. Shah and W. Aung). Wiley Interscience, New York (1987).
29. R. L. Manlapaz and S. W. Churchill, Fully developed laminar convection from a helical coil. *Chem. Engng Commun.* **9,** 185–200 (1981).
30. R. L. Manlapaz and S. W. Churchill, Fully developed laminar flow in a helically coiled tube of finite pitch, *Chem. Engng Commun.* **7,** 57–78 (1980).
31. K. Futagami and Y. Aoyama, Laminar heat transfer in a helically coiled tube, *Int. J. Heat Mass Transfer* **31**(2), 387–396 (1988).
32. G. Yang, Z. F. Dong and M. A. Ebadian, The effect of torsion on convective heat transfer in a helicoidal pipe, *J. Heat Transfer* **115,** 796–800 (1993).
33. P. Mishra and S. N. Gupta, Momentum transfer in curved pipes, *Ind. Engng Chem. Process Des. Dev.* **18**(1), 130–137 (1979).
34. S. G. R. Dennis and M. Ng, Dual solutions for steady laminar flow through a curved tube, *J. Mech. Appl. Math.* **35,** 305–324 (1982).
35. C. E. Kalb and J. D. Seader, Heat and mass transfer phenomena for viscous flow in curved circular tubes, *Int. J. Heat Mass Transfer* **15,** 801–817 (1972).
36. H. Han, Double diffusive natural convection in a vertical rectangular enclosure, Ph.D. Dissertation, University of Minnesota (1988).